

Accepted Manuscript

Synthesis and evaluation of 7-chloro-4-(piperazin-1-yl)quinoline-sulfonamide as hybrid antiprotozoal agents

Attar Salahuddin, Afreen Inam, Robyn L. van Zyl, Donovan C. Heslop, Chien-Teng Chen, Fernando Avecilla, Subhash M. Agarwal, Amir Azam

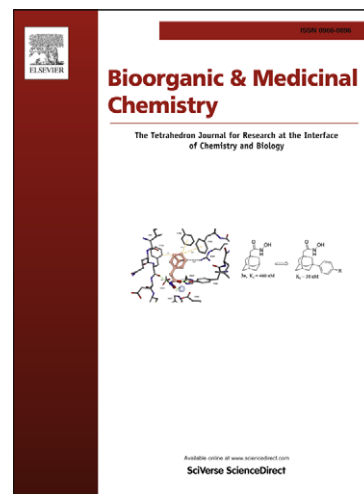
PII: S0968-0896(13)00274-5
DOI: <http://dx.doi.org/10.1016/j.bmc.2013.03.052>
Reference: BMC 10709

To appear in: *Bioorganic & Medicinal Chemistry*

Received Date: 31 January 2013
Revised Date: 16 March 2013
Accepted Date: 19 March 2013

Please cite this article as: Salahuddin, A., Inam, A., van Zyl, R.L., Heslop, D.C., Chen, C-T., Avecilla, F., Agarwal, S.M., Azam, A., Synthesis and evaluation of 7-chloro-4-(piperazin-1-yl)quinoline-sulfonamide as hybrid antiprotozoal agents, *Bioorganic & Medicinal Chemistry* (2013), doi: <http://dx.doi.org/10.1016/j.bmc.2013.03.052>

This is a PDF file of an unedited manuscript that has been accepted for publication. As a service to our customers we are providing this early version of the manuscript. The manuscript will undergo copyediting, typesetting, and review of the resulting proof before it is published in its final form. Please note that during the production process errors may be discovered which could affect the content, and all legal disclaimers that apply to the journal pertain.



Graphical Abstract

Synthesis and evaluation of 7-chloro-4-(piperazin-1-yl)quinoline-sulfonamide as hybrid antiprotozoal agents

Leave this area blank for abstract info.

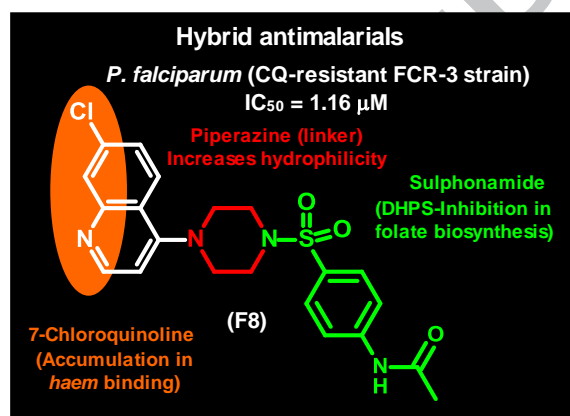
Attar Salahuddin^a, Afreen Inam^a, Robyn L. van Zyl^b, Donovan C. Heslop^b, Chien-Teng Chen^b, Fernando Avecilla^c, Subhash M. Agarwal^{d,*} and Amir Azam^{a,*}

^aDepartment of Chemistry, Jamia Millia Islamia, New Delhi-110025, India

^bPharmacology Division, Department of Pharmacy and Pharmacology, Faculty of Health Sciences, University of Witwatersrand, Johannesburg 2193, South Africa

^cDepartamento de Química Fundamental, Universidade da Coruña, Campus da Zapateira s/n, 15071, A Coruña, Spain

^dBioinformatics Division, Institute of Cytology and Preventive Oncology (ICMR), I-7, Sector-39, Noida-201301, Uttar Pradesh, India





Synthesis and evaluation of 7-chloro-4-(piperazin-1-yl)quinoline-sulfonamide as hybrid antiprotozoal agents

Attar Salahuddin^a, Afreen Inam^a, Robyn L. van Zyl^b, Donovan C. Heslop^b, Chien-Teng Chen^b, Fernando Avecilla^c, Subhash M. Agarwal^{d,*} and Amir Azam^{a,*}

^aDepartment of Chemistry, Jamia Millia Islamia, New Delhi-110025, India

^bPharmacology Division, Department of Pharmacy and Pharmacology, Faculty of Health Sciences, University of Witwatersrand, Johannesburg 2193, South Africa

^cDepartamento de Química Fundamental, Universidade da Coruña, Campus da Zapateira s/n, 15071, A Coruña, Spain

^dBioinformatics Division, Institute of Cytology and Preventive Oncology (ICMR) I-7, Sector-39, Noida -201301, Uttar Pradesh, India

ARTICLE INFO

Article history:

Received

Received in revised form

Accepted

Available online

Keywords:

Antiprotozoal agents

Sulfonamides

E. histolytica

P. falciparum

Cytotoxicity

Homology modeling

Docking

ABSTRACT

A new series of 4-aminochloroquinoline based sulfonamides were synthesized and evaluated for antiamebic and antimalarial activities. Out of the eleven compounds evaluated (F1-11), two of them (F3 and F10) showed good activity against *Entamoeba histolytica* ($IC_{50} < 5\mu M$). Three of the compounds (F5, F7 and F8) also displayed antimalarial activity against the chloroquine-resistant (FCR-3) strain of *Plasmodium falciparum* with IC_{50} values of 2 μM . Compound F7, whose crystal structure was also determined, inhibited β -haematin formation more potently than quinine. To further understand the action of hybrid molecules F7 and F8, molecular docking was carried out against the homology model of *P. falciparum* enzyme dihydropteroate synthase (PfDHPS). The complexes showed that the inhibitors place themselves nicely into the active site of the enzyme and exhibit interaction energy which is in accordance with our activity profile data. Application of Lipinski "rule of five" on all the compounds (F1-F11) suggested high drug likeness of F7 and F8, similar to quinine.

2009 Elsevier Ltd. All rights reserved.

1. Introduction

Diseases caused by protozoal organisms are responsible for considerable mortality and morbidity, affecting more than 500 million people in the world.¹ Two such protozoal diseases are malaria caused by *Plasmodium falciparum* and amoebiasis caused by *Entamoeba histolytica*.^{2,3} Malaria alone affects nearly 40% of the global population, while amoebiasis results in 50 million cases of invasive disease and up to a million fatalities per year.³ Chemotherapy remains the mainstay as the control strategy for both these diseases. 7-Chloroquinolines and nitroimidazoles as core moieties are active against malaria and amoebiasis, respectively. Chloroquinines, amodiaquine and ferroquine are the standard drugs that bear 4-aminochloroquinoline core in their structures while metronidazole, ornidazole and tinidazole are a class of nitroimidazole ring bearing drugs.

The protozoan parasites have now become resistant to some of the more effective antiprotozoal drugs, thereby pressurizing the control measures in place to treat patients infected with malaria and amoebiasis. This scenario has necessitated the search for novel drugs to contribute to the global chemotherapeutic regimens.⁴ Presently, the most promising and so far successful strategy in fighting malaria is the artemisinin combination chemotherapy (ACT), in which an artemisinin derivative is used together with conventional antimalarial drug to improve efficacy and to delay the onset of resistance.⁵ A recent rational approach of antimalarial drug design characterized as "covalent bitherapy" involves linking two molecules with individual intrinsic activity into a single agent, thus packaging dual activity into a single hybrid molecule.^{6,7} Current research in this field seems to support hybrid molecules as the next-generation antimalarial drugs, for example Trioxaferoquinines.⁶⁻⁸ Many conjugates of the available drugs for malaria have been reported since the establishment of the concept of covalent bitherapy.⁹ In many cases the conjugates have displayed more potency towards both drug resistant and non-resistant strains.

* Corresponding authors. Fax: +91 11 26980229.

E-mail addresses: amir_sumbul@yahoo.co.in (A.A),
smagarwal@yahoo.com (S.M.A)

The two enzymes DHPS (dihydropteroate synthetase) and DHFR (dihydrofolate reductase) present within folate biosynthetic pathway are ideal targets for antimicrobial therapy as folate is necessary for the cell to synthesize nucleic acids and in its absence cells is unable to divide. Sulfonamides are well known competitive inhibitors of the enzyme DHPS¹⁰ which catalyses the conversion of PABA (para-aminobenzoic acid) to dihydropteroate, a key step in folate synthesis.¹¹ Sulfadoxine is an ultra-long-lasting sulfonamide often used in combination with pyrimethamine to treat or prevent malaria.¹²

Therefore, using this recent strategy of linking two scaffolds in a single molecule, in the present study a series of novel chloroquinoline based sulfonamide hybrids were designed and evaluated for antiprotozoal activity. The design of the new hybrid molecules is illustrated (Fig. 1), whereby a 4-aminochloroquinoline was joined via a piperazine linker to a sulfonamide. It is proposed that 4-aminochloroquinoline will promote haem binding, piperazine will act as the linker and the sulfonamide group will act as a DHPS inhibitor.^{10, 13}

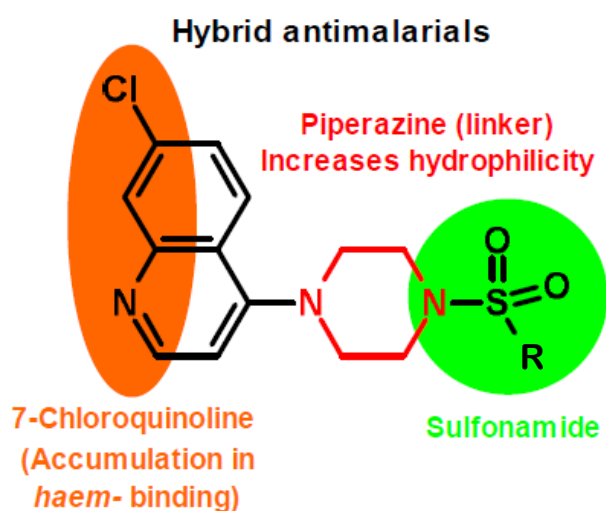


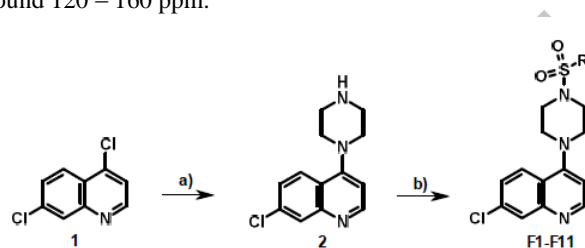
Figure 1. Rational design of hybrid antimalarials

2. Results and Discussion

2.1. Chemistry

The chloro-4-piperazin-1-yl-quinoline (2) was synthesized by aromatic nucleophilic substitution of piperazine on the commercially available 4,7-dichloroquinoline (1) under refluxing conditions in good yield. The sulfonamide formation of the final compounds (F1 to F11) was achieved by reacting 7-chloro-4-piperazin-1-yl-quinoline (2) with different sulfonyl chlorides using triethylamine as a base and dichloromethane as a solvent at 0 °C to room temperature (Scheme 1). All the products were soluble in polar solvents and recrystallization was done in dichloromethane hexane system and the compounds are stable in solid states at room temperature. Melting points were recorded on KSW melting point apparatus and are uncorrected. The ¹H NMR showed common signals of core 7-chloro-4-(piperazin-1-yl)quinoline present in all the final compounds. The C2-H is more deshielded than the C3-H due to electron withdrawing nature of the pyridine nitrogen and the electron donating capacity of piperazinyl group on the C4, and therefore appeared around δ 8.7 and 6.8, respectively. The C5-H and C6-H appeared as separate doublets around δ 7.36 and 7.76, respectively. The C8-H appeared as a singlet in all the compounds around δ 8.02. All the aromatic and aliphatic substituents in the sulfonamide group appeared as expected. The ¹³C spectra of all the compounds

showed common peaks of the core 7-chloro-4-(piperazin-1-yl)quinoline. The piperazine ring carbons showed peak around 45 and 51 ppm. Quinoline ring moiety showed peaks at 109, 121, 126 (for pyridine ring), the fused benzene part showed peaks around 120-160 ppm. The quaternary carbon attached to the piperazine showed at 135 ppm. The different aromatic sulfonyl derivatives showed their respective peaks in the aromatic region around 120 – 160 ppm.



Scheme 1. Reagents and conditions: (a) Piperazine, EtOH, reflux 12 h (77 %); b) R-Sulfonyl chlorides, Et₃N, DCM, 0°C – rt (85-95%).

2.2. Single Crystal Structure of F7

7-Chloro-4-[4-(propylsulfonyl)piperazin-1-yl]quinoline, F7, crystallizes from 30% dichloromethane/hexane solution as a colorless prism (crystal dimensions 0.22 x 0.21 x 0.20). Fig. 2 shows an ORTEP representation of F7. Hydrogen bonds were not found in the structure. Crystal data and details of the data collection and refinement for the compound F7 are mentioned in Table 1.

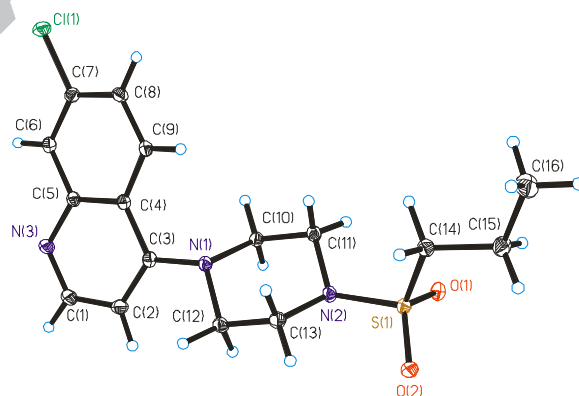


Figure 2. ORTEP plot for the compound F7. All the non-hydrogen atoms are presented by their 30% probability ellipsoids.

Table 1. Crystal data and structure refinement for F7

Compound	F7
Formula	C ₁₆ H ₂₀ ClN ₃ O ₂ S
Formula weight	353.86
T, K	100(2)
Wavelength, Å	0.71073
Crystal system	Triclinic
Space group	P $\bar{1}$
a/Å	9.4587(8)
b/Å	9.9170(9)
c/Å	10.2481(9)
α /°	90.922(7)
β /°	92.776(6)
γ /°	118.318(6)
V/Å ³	844.42(13)
Z	2
F ₀₀₀	372
D _{calc} /g cm ⁻³	1.392
μ /mm ⁻¹	0.362
θ /°	1.99 to 24.71

R_{int}	0.0662
Crystal size/ mm ³	0.22 x 0.21 x 0.20
Goodness-of-fit on F^2	1.049
R_1^a	0.0401
wR_2 (all data) ^b	0.1180
Largest differences peak and hole (e ^Å ⁻³)	0.533 and -0.392

$$^a R_1 = \frac{\sum ||F_o| - |F_c||}{\sum |F_o|}$$

$$^b wR_2 = \left\{ \frac{\sum [w(|F_o|^2 - |F_c|^2)^2]}{\sum [w(F_o^4)]} \right\}^{1/2}$$

In the crystal packing, a weak π - π stacking could account between quinoline rings [C(1)-C(2)-C(3)-C(4)-C(5)-N(3)-C(6)-C(7)-C(8)-C(9)] of an inversion-related molecules (mean separation between the quinoline rings ca 4.699 Å),¹⁴ see Fig. 3. The benzene and pyridine quinoline rings present a distortion with respect to the planarity and they are inclined at a dihedral angle of 4.95(16)^o with respect to each other. This planarity loss is related to the crystal packing forces increasing the stress of its structure. Table 2 contains selected bond lengths and angles for compound F7.

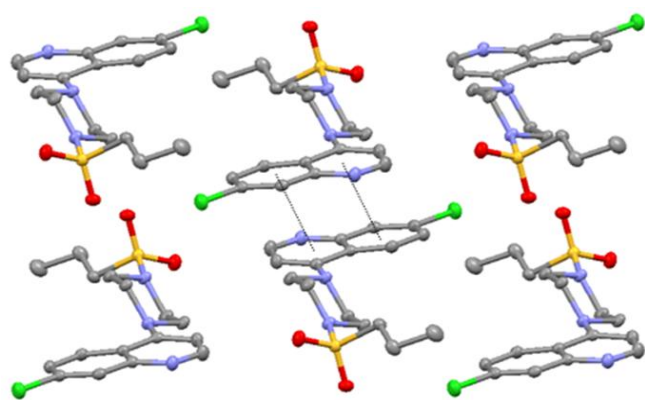


Figure 3. Crystal packing of F7. Hydrogen atoms are omitted for clarity. π - π stacking between benzene and pyridine quinoline groups are presented in dashed lines.

Table 2. Bond lengths [Å] and angles [°] for F7

Compound F7			
Bond lengths (Å)			
S(1)-O(1)	1.4330(18)	C(1)-N(3)	1.319(3)
S(1)-O(2)	1.4276(19)	N(3)-C(5)	1.375(3)
S(1)-N(2)	1.633(2)	C(4)-C(5)	1.412(4)
S(1)-C(14)	1.778(3)		
Bond Angles (°)			
N(3)-C(5)-C(4)	123.4(2)	O(2)-S(1)-O(1)	118.98(11)
C(6)-C(5)-C(4)	119.4(2)	O(1)-S(1)-N(2)	106.90(11)
C(5)-C(4)-C(3)	118.0(2)	O(2)-S(1)-N(2)	107.30(11)
C(5)-C(4)-C(9)	118.9(2)	O(2)-S(1)-C(14)	108.65(13)
		O(1)-S(1)-C(14)	107.63(12)
		N(2)-S(1)-C(14)	106.78(12)

2.3. Pharmacology

All chloroquinolinyl sulfonamides (F1-F11) were screened *in vitro* against HM1: IMSS strain of *E. histolytica* by the microdilution method.¹⁵ All the experiments were carried out in triplicate at each concentration level and repeated thrice. Cytotoxicity of active compounds has been studied using the

MTT cell viability assay on the human colon adenocarcinoma (HT29) cell line.¹⁶ *In vitro* antimalarial activity was carried out on the chloroquine-resistant (FCR-3) strain of *P. falciparum* by use of the [3H]-hypoxanthine-incorporation assay.¹⁷ To determine a possible mechanism of antimalarial action the inhibition of β -haematin formation was assessed.¹⁸ Drug toxicity was determined by examining the haemolytic effects of the compounds on healthy erythrocytes.¹⁹ The results of the experiments are summarized in Table 3.

2.3.1 Antiamoebic activity

Preliminary experiments were carried out to determine the *in vitro* antiamoebic activity of all the compounds (F1-F11) by microdilution method using the HM1: IMSS strain of *E. histolytica*. The antiamoebic effect was compared with the most widely used antiamoebic medication, namely metronidazole which had a 50% inhibitory concentration (IC₅₀) of 1.46 μ M (Table 3). The structure activity relationship (SAR) showed that compounds (F1-F11) which contained aliphatic substituents in the benzene ring of the sulfonamide group increased with the increasing hydrophobicity, hence F3 (IC₅₀: 2.86 μ M) with the most bulky and hydrophobic t-butyl group showed highest antiamoebic activity, while F10 (IC₅₀: 4.54 μ M) with a p-tolyl sulfonamide group showed considerable activity (Fig. 4). The compounds F4 (IC₅₀: 8.23 μ M) and F8 (IC₅₀: 9.61 μ M) with a para substitution in the benzene ring of the sulfonamide group have comparatively less IC₅₀ values than the other substituted compounds (Fig. 4). Aliphatic sulfonamide F7 (IC₅₀: >100 μ M) and F11 (IC₅₀: >100 μ M) were found to be the least active compounds in the series. Therefore it was concluded that for display of antiamoebic activity, an aromatic sulfonamide with aliphatic/hydrophobic substitutions at para position is required in the final structure of 7-chloro-4-piperazin-1-yl-quinoline sulfonamides. Collectively only one compound F3 (IC₅₀: 2.86 μ M) was found to be nearly as active to the standard drug metronidazole (IC₅₀: 1.46 μ M).

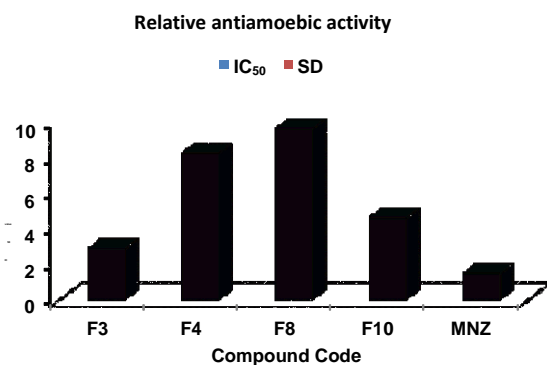


Figure 4. Relative antiamoebic activities

2.3.2 Antimalarial, haemolytic and β -haematin inhibitory activity

The series of chloroquinolinyl piperazine sulfonamides (F1-F11) were examined for their *in vitro* antimalarial activity, haemolytic properties and to elucidate a possible mechanism of action, their ability to inhibit the formation of β -haematin was also assessed (Table 3). In contrast to the activity observed against *Entamoeba*, where compounds F3 and F10 were the most active, compounds F8, F7 and F5 were the most active against *Plasmodium falciparum* with IC₅₀ values less than 2 μ M. None of the compounds caused significant haemolysis of the uninfected human erythrocytes, thus, indicating that the compounds entered the parasite and directly inhibited parasite growth, rather than

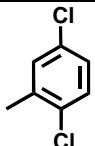
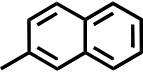
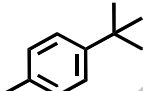
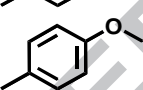
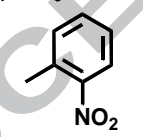
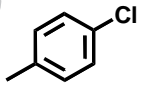
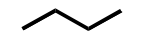
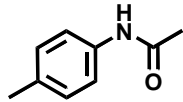
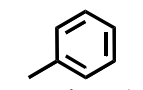
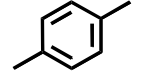
interfering with the red blood cell membrane integrity. The *N*-acetylaniline substitution in compound F8 (4-[[4-(7-chloroquinolin-4-yl)piperazin-1-yl]sulfonyl]-*N*-acetylaniline) was the most active in the series, although activity was at least 7 fold less than the standard antimalarial agent, quinine. The decrease in inhibitory activity can be attributed to the sulfonamide/sulfadoxine group, which against this *Plasmodium* strain has an IC_{50} value of greater than 100 μ M. Thus, it does not contribute to the overall antimalarial activity of the new complex. Although the antimalarial activity of the compounds did not correlate with their ability to inhibit β -haematin formation, several structures did display interesting properties to be used as lead compounds to improve upon the antimalarial efficacy. Namely, the ability of a compound F8 to inhibit β -haematin formation ($IC_{50} = 8.84\mu$ M) as potently as chloroquine, a known inhibitor of β -haematin formation (IC_{50} value: $8.63 \pm 2.13 \mu$ M), which could indicate one possible mechanism of action of this compound. In contrast, although the nitrophenyl group on the benzene ring of compound F5 retained the compounds activity against the intra-erythrocytic parasite, its ability to inhibit β -haematin formation was not comparable to that of chloroquine or quinine (Table 3). The aliphatic propyl group substituted on the

benzene ring (compound F7) not only increased the antimalarial activity when compared to the methyl substitution (compound F11), but it also increased the ability of the compound to inhibit β -haematin formation.

2.3.3 Cytotoxicity profile

Overall, the compounds inhibited approximately 30% cell viability at 100 μ M, with compound F8 being the least toxic (Table 3). In contrast, compound F9 was the most inhibitory against the colon adenocarcinoma by inhibiting 45% cell growth, in comparison to 52% by camptothecin (CTT), a cytotoxic quinoline alkaloid which inhibits the DNA enzyme, topoisomerase I.²⁰ The two most active compounds against amoebiasis, compounds F3 and F10, had a safety index of 24 and 14, respectively. The three most active compounds against *P. falciparum*, compounds F8, F7 and F5, were relatively non-toxic to the colon adenocarcinoma cells, where overall 17% of cells were inhibited at 100 μ M. The safety index of these three compounds was 84, 39 and 44, respectively.

Table 3. Biological activity results

Compd	R-substitution	Antiamoebic activity (HM1:IMSS)	Antimalarial activity (FCR-3)	Haemolytic activity	Inhibition of β -haematin formation	Cytotoxicity (HT29)
		$IC_{50} \pm$ S.D. (μ M)	$IC_{50} \pm$ S.D. (μ M)	% Lysis \pm S.D. at 100 μ M	$IC_{50} \pm$ S.D. (μ M)	% Cell viability \pm S.D. at 100 μ M
F1		30.2 ± 0.23	2.55 ± 0.38	2.06 ± 0.46	47.22 ± 3.67	63.39 ± 9.57
F2		23.4 ± 0.02	3.06 ± 0.59	0.97 ± 0.01	71.17 ± 5.60	59.76 ± 2.76
F3		2.86 ± 0.03	6.09 ± 0.30	1.36 ± 0.32	72.40 ± 1.93	67.69 ± 7.74
F4		8.23 ± 0.012	3.30 ± 0.31	6.03 ± 0.11	9.04 ± 1.90	68.11 ± 19.15
F5		$>100 \pm 0.9$	1.94 ± 0.37	0.01 ± 0.01	63.54 ± 1.82	86.11 ± 14.12
F6		25.7 ± 0.1	3.27 ± 0.23	1.40 ± 0.18	34.77 ± 0.66	61.27 ± 12.58
F7		$>100 \pm 0.91$	1.72 ± 0.22	0.82 ± 0.20	1.79 ± 0.22	67.07 ± 12.01
F8		9.61 ± 0.02	1.16 ± 0.36	0.83 ± 0.12	8.84 ± 1.27	96.84 ± 11.20
F9		32.8 ± 0.26	4.02 ± 1.00	0.01 ± 0.01	18.09 ± 4.05	55.15 ± 17.42
F10		4.54 ± 0.1	4.22 ± 0.62	0.62 ± 0.13	8.92 ± 2.39	64.45 ± 12.66
F11	CH ₃	$>100 \pm 0.21$	8.54 ± 1.49	0.01 ± 0.01	13.54 ± 1.73	72.96 ± 14.55
(MNZ)	Metronidazole	1.45 ± 0.06	N.D.	N.D.	N.D.	N.D.
Qu.	Quinine	N.D.	0.17 ± 0.03	2.14 ± 0.34	22.08 ± 3.10	N.D.

CTT	Camptothecin	N.D.	N.D.	N.D.	N.D.	48.33 ± 4.18
-----	--------------	------	------	------	------	--------------

2.4. Measuring drug-likeness

Good bioavailability can be achieved with a balance between solubility and partitioning properties. Thus in order to gain insight into the drug likeness of our compounds in comparison to standard drugs we subjected the compounds F1-F11 for the prediction of lipophilicity and Lipinski's "Rule of Five".²¹ High oral bioavailability is an important factor for the development of bioactive molecules as therapeutic agents. Good intestinal absorption, reduced molecular flexibility (measured by the number of rotatable bonds), low polar surface area (PSA) or total hydrogen bond count (sum of donors, HBDs and acceptors, HBAs), are important predictors of good oral bioavailability.²² Molecular properties such as membrane permeability and bioavailability are associated with log P (partition coefficient), molecular weight (MW), or hydrogen bond acceptors and donors count in a molecule.²³ The rule states that most molecules with good membrane permeability have log P <5, molecular weight <500, number of hydrogen bond acceptors <10, and number of hydrogen bond donors <5. This rule is widely used as a filter for drug-like properties. An analysis of small drug-like molecules suggests a filter of log D > 0 and <3, which enhances the probability of a compound to exhibit good intestinal permeability. A poor permeation or absorption is more likely when there are more than 5 H-bond donors and 10 H-bond acceptors. All the compounds (F1-F11), quinine and chloroquine have obeyed the "Rule of Five" with logP values <5 and HBA ≤5. All the compounds (F1-F11) under investigation possess hydrogen bond donor's ≤1 and a considerable number of hydrogen bond acceptors (≤5) as shown in Table 4. The most active compounds against *P. falciparum* F7 and F8 have peculiar properties with log P values nearly equal to that of quinine. F7 has a PSA near to that of quinine, while F8 has distinctly large PSA value.

Table 4. Lipinski tools for measuring drug likeness

No.	Mol.wt	LogP	Log D	No of HBAs*	No of HBDs*	PSA
F1	456.773	4.73	4.54	4	0	53.51
F2	437.942	4.52	4.32	4	0	53.51
F3	443.989	5.07	4.88	4	0	53.51
F4	417.909	3.37	3.18	5	0	62.74/
F5	432.881	3.47	3.28	5	0	99.33
F6	422.328	4.13	3.94	4	0	53.51
F7	353.867	2.44	2.25	4	0	53.51
F8	444.934	2.76	2.57	5	1	82.61
F9	387.883	3.53	3.34	4	0	53.51
F10	401.910	4.04	3.85	4	0	53.51
F11	325.814	1.41	1.22	4	0	53.51
CHQ	325.814	3.93	0.88	3	1	28.16
QU	324.416	2.51	0.86	4	1	45.59

*HBA- hydrogen bond acceptor, HBD-Hydrogen bond donor, PSA-polar surface area obtained by Marvin Sketch 5.1

A graph of IC₅₀ versus the logP values clearly indicates that F7 and F8 have high drug-likeness similar to chloroquine and quinine. F7, F8 and standard drugs used have high proximity therefore lie near the Y-axis with low IC₅₀ and logP values (circled) (Fig. 5)

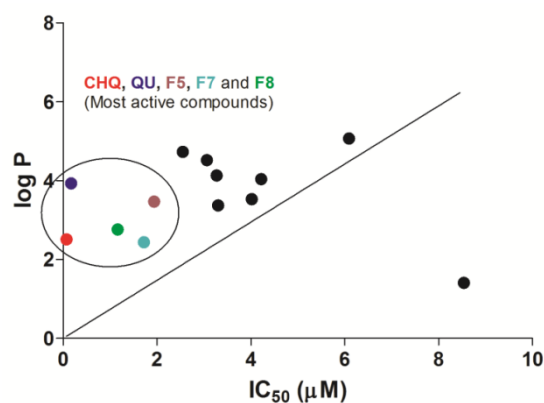


Figure 5. Graph showing correlation between log P and IC₅₀ values for *P. falciparum* growth inhibition by F1-F11, chloroquine and quinine. The compounds whose log P values are close to the linear line and have lower IC₅₀ values are the most active. The most active compounds are encircled.

2.5. Comparative modeling of PfDHP

As we have designed hybrid molecules capable of exhibiting dual activity i.e. β-haematin and DHPS inhibition, we also generated a homology model of PfDHPS so as to analyze the interactions of the quinoline based sulfonamides with the enzyme. To construct the 3D model of PfDHPS, a BLAST search was performed against the Protein Data Bank (PDB)²⁴ for template identification. BLAST analysis revealed that Bacillus anthracis DHPS (PDB code 1TX0) shares 35% identity and 49% similarity, the highest with PfDHPS and therefore it was selected as the template for model construction. The sequence alignment of the 1TX0 with PfDHPS sequence that was used for model construction is shown in Fig. 6. Homology modeling was then carried out through Modeller 9v9.²⁵ The constructed model was then subjected to loop refinement followed by energy minimization. The stereo chemical quality of the final predicted structure was assessed using PROCHECK²⁶, which showed that 84.1% of the residues were in the 'most favored region' and 15.4% in the combined 'allowed region' and one residue (Asp110) was found in the disallowed region. Also, it is established that the score for G-factors should be above -0.50 for a reliable model.²⁷ We observed that the G-factor scores of the model was -0.22 for dihedral bonds, 0.06 for covalent bonds and -0.09 overall. The distribution of the main chain bond lengths and bond angles was 99.9% and 93.0% within limits. The quality of the structure is further evident by the fact that according to VERIFY3D²⁸, 82.33% of the residues have a score of greater than 0.2, which indicates a good quality model.

PfDHPS	1	EKTNIVGILNVNYSFSDGGIFVEPKRAVQRMFEMINEGASVIDIGGESSAPFVIPNPKI	60
		EKT I+GILNV DSFSDGG + E AV+ EM +EGA +IDIGGES+ P	
1TX0	1	EKTLIMGILNVTPDSFSDGGSYNEVDAAVRHAKEMRDEGAHIIDIGGESTRPGFAKVSVE	60
PfDHPS	61	SERDLVVPVLQQLFQKEWNDIKNKIVKCDAKPIISIDTINYNVFKECVDNDLVDILNDISA	120
		E VVP++Q KE K ISIDT V K+ ++ I+NDI	
1TX0	61	EEIKRVVPMIQAVSKE-----VKLPISIDTYKAEVAKQAIEAG-AHIINDIWG	107
PfDHPS	121	CTNNPEIILKLLKKNKFYSVVLHMKRGNPHTMDKLTNYDNLVYDIKNYLEQRLNFLVLNG	180
		P+I ++ + ++LMH R N NY NL+ D+ L + G	
1TX0	108	AKAEPKIAEVAAHYD--VPIILMHNDRN-----MNYRNLMDMIADLYDSIKIAKDG	158
PfDHPS	181	IPRYRILFDIGLGFQAKHDQSIKLLQNIHVYD--EYPLFIGYSRKRFFIAHCMN	231
		+ I+ D G+GFAK +Q+++ ++N+ + YP+ +G SRK FI H ++	
1TX0	159	VRDENIILDPGIGFAKTPEQNLEAMRNLEQLNVLGYPVLLGTSTRKSFIGHVLD	211

Figure 6. Sequence alignment of PfDHPS with the template (Pdb id: 1TX0)

Also we analyzed the model using ProSA-web²⁹ which measures the z-score (indicating overall model quality) and deviation of the total energy of the structure with respect to energy distribution derived from random conformations. The overall ProSA z-score evaluated for the model developed in this study was -7.29, which is comparable to X-ray crystallized template structure of 1TX0 (z-score = -7.71). Further, the root-mean-square deviation (RMSD) between the backbone atoms of the template and the homology model was observed to be 0.734 Å indicating reasonably good structural parameters of the predicted structure (Fig. 7).

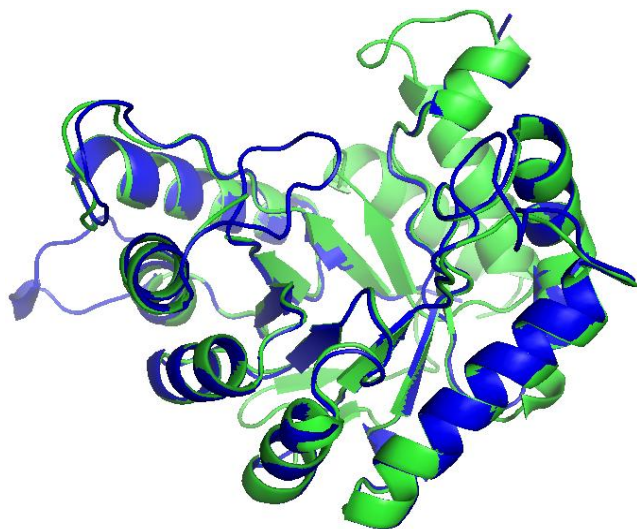
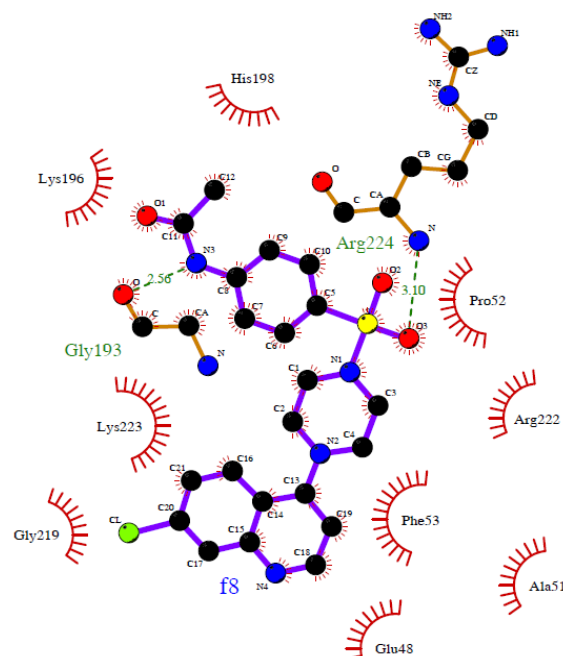


Figure 7. Structural superimposition of Ca trace of PfDHPS model (represented in blue color) with known crystal structure (represented in green color). The root-mean-square deviation (RMSD) between the template and the homology model was 0.734 Å

2.6. Molecular docking

After the homology model was constructed, the active site information was obtained by superimposing 3-D structure of the PfDHPS with that of *E. coli* DHPS (Pdb id: 1AJ0), as it contains sulfonamide bound in the active site. Thereafter, docking in the binding pocket of the modeled protein was undertaken using Autodock 4.2³⁰ and the interacting residues with two most promising *P. falciparum* inhibitors (F7 and F8) were determined. It was noted that Autodock binding energy of F7 and F8 was -7.37 and -7.89 with PfDHPS respectively, which is in accordance with our activity profile data that indicated F8 to be the most active inhibitor of *Plasmodium* growth, followed by F7. Ligplot³¹ analysis of docked complex

with F8 reveals that the residues Glu 48, Ala 51, Pro 52, Phe 53, Lys 196, His 198, Gly 219, Arg 222 and Lys 223 are involved in hydrophobic interaction, while Gly 193 and Arg 224 forms hydrogen bond with N3 and O3 of F8, respectively (Fig. 8a). Previously too, *P. falciparum* DHPS homology modeling followed by molecular docking has demonstrated that sulfadoxine docks into the same active site having similar active site forming residues in interaction with the inhibitor.³² Further, we observe that F7 also interacts with similar residues (Ala 51, Pro 52, Phe 53, Gly 193, Lys 196, Lys 197, His 193 and Phe 225) that contribute towards a hydrophobic interaction and exhibits hydrogen bond with Arg 224 (Fig. 8b). Thus the docking studies are in concurrence with previous studies and provide additional evidence that these compounds may inhibit the growth of *P. falciparum* by interacting with PfDHPS.



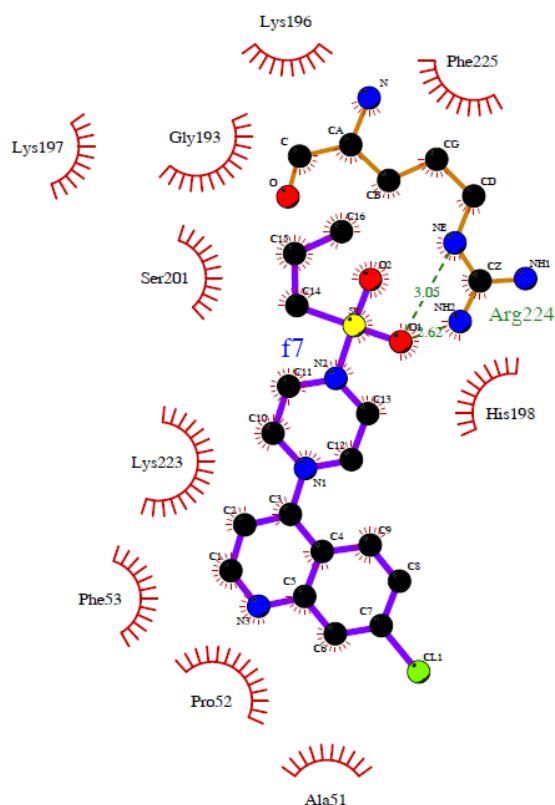


Figure 8. Schematic 2D representation of interactions of (a) F8 and (b) F7. Hydrogen bonds are shown with green dashed lines, and hydrophobic contacts by red arcs with radiating lines.

3. Conclusions

The present study indicates that the complex consisting of 4-aminochloroquinoline and sulfadoxine linked via piperazine is a viable combination as it acts against both *Entamoeba histolytica* and *Plasmodium falciparum*. Overall, the compounds F3 (7-chloro-4-{4-[(4-t-butylphenyl)sulfonyl]piperazin-1-yl}quinoline) and F8 ((4-{[4-(7-chloroquinolin-4-yl)piperazin-1-yl]sulfonyl}-N-acetylaniline)) which possess favourable structural features need to be further developed to increase antiamoebiasis and antiplasmodial activity respectively.

4. Experimental Section

4.1. Chemistry

All the required chemicals were purchased from Merck and Aldrich Chemical Company (USA). Precoated aluminium sheets (silica gel 60 F₂₅₄, Merck Germany) were used for thin-layer chromatography (TLC) and spots were visualized under UV light. Elemental analysis was carried out on CHNS Elementar (Vario EL-III) and the results were within $\pm 0.3\%$ of the theoretical values. IR spectra were recorded on Bruker FT-IR spectrophotometer under neat condition on ZnSe Crystal. ¹H NMR and ¹³C NMR spectra were recorded on Bruker Spectrospin DPX 300 MHz spectrometer, respectively using CDCl₃ as a solvent and trimethylsilane (TMS) as an internal standard. Splitting patterns are designated as follows: s, singlet; d, doublet; m, multiplet. Chemical shift values are given in ppm. The FAB mass spectra of the compounds were recorded on JEOL SX 102/DA-6000 mass spectrometer using Argon/Xenon (6 KV, 10 mA) as the FAB gas and m-nitrobenzyl alcohol (NBA) was used as the matrix.

4.1.1 7-Chloro-4-piperazin-1-yl-quinoline (2).

To a stirred solution of 4,7-dichloroquinoline (1) (10 g, 50.49 mmol) in 150 mL ethanol was added piperazine (30.44 g, 353.44 mmol), the resulting solution was then refluxed for 12 h. On reaction completion (TLC) the reaction was then concentrated under vacuum to give a crude solid mixture which was taken up in 200 mL DCM and washed with saturated sodium bicarbonate solution until no piperazine was seen in the organic layer (TLC). The combined organic extracts were dried over anhydrous sodium sulfate and concentrated to give a crude product which was purified by recrystallization in 30% DCM: Hexane as a white powder (9.7 g, 77.6%) of compound 2.: R_f = 0.25 (10% MeOH/CHCl₃) mp: 118-120 °C; Anal. calc. for C₁₃H₁₄ClN₃: C 63.03, H 5.70 N 16.96 % found: C 63.23, H 5.61, N 17.02 %; IR ν_{max} (cm⁻¹): 1652 (C=O), 1579 (C=C); ¹H NMR (CDCl₃) δ(ppm): 3.14-3.21(m, 8H), 3.33 (s, 1H), 6.83 (d, 1H J=5.1Hz), 7.42 (dd, 1H, J=2.1Hz and 9Hz), 7.97 (t, 1H, J=9Hz) 8.06 (dd, 1H, J=2.1Hz and 9Hz), 8.72 (d, 1H, J=5.1 Hz); FAB-MS (m/z): [M⁺+1] 248

4.1.2 7-Chloro-4-(4-Alkyl/Aryl sulfonyl-piperazin-1-yl)-quinoline (F1 to F11).

To a stirred solution of 7-chloro-4-piperazin-1-yl-quinoline (2) (0.25 g, 1 mmol) in 8-10 mL of DCM at 0 °C was added triethylamine (0.12 mL, 1.26 mmol). Different aryl sulfonyl chlorides (1 mmol) were added dropwise / portion wise and the resulting solution was stirred further for 15 min at 0 °C and then stirred at room temperature for different time intervals. On reaction completion (TLC), the reaction mix was diluted with 20 mL water and 20 mL DCM and partitioned in separating funnel, where the organic layer was washed with water (3x 20 mL) before being separated and dried over sodium sulfate to yield compound 3 in which was recrystallized in DCM:Hexane to yield pure products in 85-95% yields.

4.1.3 7-Chloro-4-[4-[(2,5-dichlorophenyl)sulfonyl] piperazin-1-yl] quinoline (F1)

Yield 95%; (DCM/Hexane); R_f = 0.65 (5% MeOH/CHCl₃) mp: 165-167°C; Anal. calc. for C₁₉H₁₆Cl₃N₃O₂S: C 49.96, H 3.53, N 9.20, S 7.02% found: C 49.7, H 3.32, N 9.25, S 7.2%. IR ν_{max} (cm⁻¹): 1569.29, 1157.53, 1034.73, 817.46, 575.83, 671.67. ¹H NMR (CDCl₃) δ(ppm): 3.254 (t, 4H, J=3.3Hz), 3.613 (t, 4H, J=3.3Hz), 6.849 (d, 1H, J=4.8Hz), 7.424 (d, 1H, J=9Hz), 7.509 (s, 2H), 7.863 (d, 1H, J=8.7Hz), 8.072 (d, 2H, J=15.6), 8.743 (d, 1H, J=4.8Hz). ¹³C NMR δ (ppm): 45.76, 51.95, 109.50, 121.67, 124.51, 126.64, 129.04, 130.46, 131.80, 133.31, 133.35, 135.14, 137.39, 150.05, 151.90, 156.06. FAB-MS (m/z): [M⁺+1] 456.25

4.1.4 7-Chloro-4-[4-(2-naphthylsulfonyl)piperazin-1-yl]quinoline (F2)

Yield: 93%,(DCM/Hexane): R_f = 0.6 (5% MeOH/CHCl₃) m.p.: 179-182°C; Anal. Calc. for C₂₃H₂₀ClN₃O₂S: C 63.08, H 4.60, N 9.59, S 7.32%; found: C 62.89, H 4.71, N 9.44, S 7.3%. IR ν_{max} (cm⁻¹): 1569.36, 1160.65, 1069.27, 818.68, 571.09, 606.33, 646.23; ¹H NMR (CDCl₃) δ(ppm): 3.29 (t, 4H, J = 4.2Hz), 3.38 (t, 4H, J=4.2Hz), 6.851 (d, 1H, J=4.8Hz), 7.31-7.35 (dd, 1H, J = 2.1 & 9Hz), 7.64-7.73 (m, 3H), 7.81-7.85 (dd, 1H, J=1.8 & 8.7Hz), 7.96-8.09 (m, 4H), 8.42 (s, 1H), 8.72 (d, 1H, J=4.8Hz); ¹³C NMR (CDCl₃) δ(ppm): 46.03, 51.46, 109.36, 121.52, 122.83, 124.53, 126.46, 127.73, 127.96, 128.83, 129.05, 129.18, 129.21, 129.46, 132.15, 132.36, 134.95, 135.04, 149.82, 151.78, 156.00; FAB-MS (m/z): [M⁺+1] 438.

4.1.5 7-Chloro-4-[4-[(4-*t*-butylphenyl)sulfonyl]piperazin-1-yl]quinoline (F3)

Yield: 91%, (DCM/Hexane); $R_f = 0.7$ (5% MeOH/CHCl₃) m.p.: 170-173°C; Anal. Calc. for C₂₃H₂₆ClN₃O₂S: C 62.22, H 5.90, N 9.46, S 7.22%; found: C 62.3, H 5.72, N 9.56, S 7.13%. IR ν_{\max} (cm⁻¹): 1569.33, 1163.35, 832.21, 578.93, 611.72, 2962.37, 942.08; ¹H NMR (CDCl₃) δ (ppm): 1.385 (s, 9H), 3.315 (d, 8H, J=4.5Hz), 6.853 (d, 1H, J=5.1Hz), 7.362-7.398 (d, 1H, J=1.8 & 8.85Hz), 7.612 (d, 2H, J=8.4Hz), 7.772 (m, 3H), 8.031 (d, 1H, J=1.8Hz), 8.720 (s, 1H); ¹³C NMR (CDCl₃) δ (ppm): 31.10, 35.26, 45.79, 45.98, 51.57, 109.45, 121.62, 124.64, 126.30, 126.55, 127.73, 128.98, 132.42, 135.11, 149.98, 151.93, 156.13, 157.02. FAB-MS (m/z): [M⁺+1] 444.39

4.1.6 7-Chloro-4-[4-[(4-methoxyphenyl)sulfonyl]piperazin-1-yl]quinoline (F4)

Yield: 90%, (Dull white solid, DCM/Hexane), $R_f = 0.6$ (5% MeOH/CHCl₃) m.p.: 220-223°C; Anal. calc. for C₂₀H₂₀ClN₃O₃S: C 57.48, H 4.82, N 10.05, S 7.67%; found: C 57.32, H 4.94, N 10.02, S 7.37%; IR ν_{\max} (cm⁻¹): 1571.59, 1189.23, 1156.81, 1063.59, 823.62, 550.33, 653.20, 608.15, 1253.95; ¹H NMR (CDCl₃) δ (ppm): 3.288 (s, 8H), 3.194 (s, 3H), 6.843 (d, 1H, J=1.6Hz), 7.073 (d, 2H, J=8.4Hz), 7.375 (d, 1H, J=9Hz), 7.75-7.79 (m, 3H), 8.029 (s, 1H), 8.73 (d, 1H, J=4.8Hz); ¹³C NMR (CDCl₃) δ (ppm): 46.05, 51.51, 55.72, 109.47, 114.47, 121.67, 124.65, 126.53, 126.84, 129.04, 130.00, 135.09, 150.05, 151.98, 156.09, 163.33. FAB-MS (m/z): [M⁺+1] 418.12

4.1.7 7-Chloro-4-[4-[(2-nitrophenyl)sulfonyl]piperazin-1-yl]quinoline (F5)

Yield: 94%, (Off white solid, DCM/Hexane), $R_f = 0.5$ (5% MeOH/CHCl₃) m.p.: 152-155°C; Anal. calc. for C₁₉H₁₇ClN₄O₄S: C 52.72, H 3.96, N 12.94, S 7.41%; found: C 52.63, H 3.77, N 12.91, S 7.33%. IR ν_{\max} (cm⁻¹): 1546.68, 1165.92, 1012.97, 814.70, 569.42, 696.93, 611.15, 859.81, 1546.63, 1350.76; ¹H NMR (CDCl₃) δ (ppm): 3.282 (t, 4H, J=4.5Hz), 3.615 (t, 4H, J=4.8Hz), 6.851 (d, 1H, J=5.1Hz), 7.40-7.43 (dd, 1H, J=1.8 & 9Hz), 7.65-7.70 (m, 1H), 7.72-7.80 (m, 2H), 7.85 (d, 1H, J=9Hz), 8.03-8.06 (dd, 2H, J = 1.8 & 6.6Hz), 8.74 (d, 1H, J=5.1Hz); ¹³C NMR (CDCl₃) δ (ppm): 45.95, 51.84, 109.60, 121.73, 124.30, 124.60, 126.69, 129.09, 130.98, 131.09, 131.78, 134.12, 135.17, 148.44, 150.10, 152.00, 156.07. FAB-MS (m/z): [M⁺+1] 433.3

4.1.8 7-Chloro-4-[4-[(4-chlorophenyl)sulfonyl]piperazin-1-yl]quinoline (F6)

Yield: 93.3%, (White solid, DCM/Hexane), $R_f = 0.65$ (5% MeOH/CHCl₃) m.p.: 164-167°C; Anal. calc. for C₁₉H₁₇Cl₂N₃O₂S: C 54.04, H 4.06, N 9.95, S 7.59%; found: C 54.22, H 4.3, N 9.52, S 7.43%; IR ν_{\max} (cm⁻¹): 1571.66, 1340.79, 1162.67, 607.60, 759.46, 815.34, 1259.38; ¹H NMR (CDCl₃) δ (ppm): 3.299 (m, 8H), 6.843 (d, 1H, J=4.8Hz), 7.396-7.359 (dd, 1H, J=2.1 & 9Hz), 7.588 (d, 2H, J=8.7Hz), 7.79-7.74 (m, 3H), 8.301 (d, 1H, J=1.8Hz), 8.726 (s, 1H); ¹³C NMR (CDCl₃) δ (ppm): 45.95, 57.42, 109.46, 121.58, 124.48, 126.55, 129.02, 129.15, 129.61, 133.91, 135.08, 150.00, 151.92, 155.88; FAB-MS (m/z): [M⁺+1] 423.4

4.1.9 (7-Chloro-4-[4-(propylsulfonyl)piperazin-1-yl]quinoline (F7)

Yield: 94.8%, (Pale yellow solid, DCM/Hexane), $R_f = 0.55$ (5% MeOH/CHCl₃) m.p.: 118-121°C; Anal. calc. for C₁₆H₂₀ClN₃O₂S: C 54.31, H 5.70, N 11.87, S 9.06%; found: C

54.39, H 5.73, N 11.66, S 9.11 %; IR ν_{\max} (cm⁻¹): 1579.55, 1258.12, 1373.47, 1152.19, 1492.81, 826.67, 608.37; ¹H NMR (CDCl₃) δ (ppm): 1.11 (t, 3H, J=14.7Hz), 1.927 (m, 2H), 2.99 (t, 2H, J=15.6Hz), 3.277 (t, 4H, J=9Hz), 3.5 (t, 4H, J=9Hz), 6.86 (d, 1H, J=4.8Hz), 7.42-7.46 (dd, 1H, J=11.8 & 9Hz), 7.95 (d, 1H, J=9Hz), 8.053 (d, 1H, J=1.5Hz), 8.749 (d, 1H, J=5.1Hz); ¹³C NMR (CDCl₃) δ (ppm): 13.10, 16.78, 45.64, 51.13, 51.98, 109.46, 121.65, 124.54, 126.52, 128.96, 135.00, 150.00, 151.89, 156.89, 156.07; FAB-MS (m/z): [M⁺+1] 354.2

4.1.10 4-[[4-(7-Chloroquinolin-4-yl)piperazin-1-yl]sulfonyl]-N-acetylaniline (F8)

Yield: 82.4%, (White solid, DCM/Hexane), $R_f = 0.75$ (5% MeOH/CHCl₃) m.p.: 265-268°C; Anal. calc. for C₂₁H₂₁ClN₄O₃S: C 56.69, H 4.76, N 12.59, S 7.21%; found: C 59.87, H 4.71, N 12.44, S 7.12%; IR ν_{\max} (cm⁻¹): 3186.04, 1669.62, 13340.60, 1158.41, 1262.29, 829.51, 608.82; ¹H NMR (CDCl₃) δ (ppm): 2.263 (s, 3H), 3.300 (s, 8H), 6.862 (d, 1H, J=4.8Hz), 7.391-7.49 (dd, 1H, J=2.1 & 9Hz), 7.776-7.824 (m, 5H), 8.042 (d, 1H, J=1.8Hz), 8.199 (s, 1H), 8.747 (d, 1H, J=4.8Hz); ¹³C NMR (CDCl₃) δ (ppm): 24.33, 45.88, 51.28, 53.36, 108.82, 109.48, 119.53, 121.71, 124.69, 126.61, 128.98, 129.03, 135.15, 150.05, 151.96, 156.11; FAB-MS (m/z): [M⁺+1] 445.2

4.1.11 7-Chloro-4-[4-(phenylsulfonyl)piperazin-1-yl]quinoline (F9)

Yield: 85.6%, (Dark brown solid, DCM/Hexane), $R_f = 0.6$ (5% MeOH/CHCl₃) m.p.: 148-151°C; Anal. calc. for C₁₉H₁₈ClN₃O₂S: C 58.83, H 4.68, N 10.83, S 8.27%; found: C 58.8, H 4.62, N 10.68, S 8.21%. IR ν_{\max} (cm⁻¹): 1337.20, 1158.52, 1237.26, 813.19, 733.44, 606.73; ¹H NMR (CDCl₃) δ (ppm): 3.32-3.34 (m, 4H), 3.41-3.42 (m, 4H), 6.90 (d, 1H, J=5.4Hz), 7.39-7.43 (dd, 1H, J=2.1 & 8.85Hz), 7.55-7.78 (m, 3H), 7.76 (d, 1H, J=9Hz), 7.75-7.85 (m, 2H), 8.12 (d, 1H, J=2.1Hz), 8.73 (d, 1H, J=5.4Hz); ¹³C NMR (CDCl₃) δ (ppm): 45.92, 45.98, 51.54, 108.98, 120.96, 124.93, 125.97, 127.03, 127.81, 128.31, 133.36, 135.36, 136.33, 150.13, 157.24. FAB-MS (m/z): [M⁺+1] 388.16

4.1.12 7-Chloro-4-[4-[(4-methylphenyl)sulfonyl]piperazin-1-yl]quinoline (F10)

yield: 80.2%, (Light brown solid, DCM/Hexane) $R_f = 0.7$ (5% MeOH/CHCl₃) m.p.: 172-175°C; Anal. calc. for C₂₀H₂₀ClN₃O₂S: C 59.77, H 5.02, N 10.45, S 7.98%; found: C 59.68, H 5.18, N 10.6, S 8.0%. IR ν_{\max} (cm⁻¹): 1570.29, 1011.62, 1336.34, 1157.93, 867.99, 812.82, 610.28; ¹H NMR (CDCl₃) δ (ppm): 2.485 (s, 3H), 3.296 (s, 8H), 6.843 (d, 1H, J=5.1Hz), 7.36-7.42 (m, 3H), 7.71-7.77 (m, 3H), 8.037 (d, 1H, J=1.8Hz), 8.731 (d, 1H, J=6.9Hz); ¹³C NMR (CDCl₃) δ (ppm): 21.55, 45.95, 51.44, 109.36, 121.55, 124.57, 126.44, 127.79, 128.88, 129.85, 132.29, 135.03, 144.05, 149.88, 151.81, 156.04; FAB-MS (m/z): [M⁺+1] 402.1

4.1.13 7-Chloro-4-[4-(methylsulfonyl)piperazin-1-yl]quinoline (F11)

Yield: 91.3%, (Pale yellow solid, DCM/Hexane), $R_f = 0.45$ (5% MeOH/CHCl₃) m.p.: 197-200 °C Anal. calc. for C₁₄H₁₆ClN₃O₂S: C 51.61, H 4.95, N 12.90, S 9.84%; found: C 51.39 H 4.9, N 12.88, S 9.81%. IR ν_{\max} (cm⁻¹): 1592.25, 1332.69, 1155.43, 815.32, 609.39; ¹H NMR (CDCl₃) δ (ppm): 2.924 (s, 3H), 3.88 (t, 4H, J=9Hz), 3.554 (t, 4H, J=9Hz), 6.69 (d, 1H, J=5.1Hz), 7.46-7.50 (dd, 1H, J=2.1 & 9Hz), 7.931 (d, 1H, J=9Hz), 8.09 (s, 1H), 8.776 (d, 1H, J=5.1Hz); ¹³C NMR (CDCl₃) δ (ppm): 34.82, 45.77, 51.71, 109.41, 121.52, 124.61,

126.79, 128.6, 135.51, 149.47, 151.46, 156.39; FAB-MS (m/z): [M⁺+1] 326.41

4.2. *In vitro* antiamoebic assay

All the compounds (F1- F11) were screened *in vitro* for antiamoebic activity against HM1: IMSS strain of *E. histolytica* by a microdilution method.¹⁵ *E. histolytica* trophozoites were cultured in a 96-well microtiter plate suspended in Diamond TYIS-33 growth medium.³³ The test compounds (1 mg) were dissolved in DMSO (40 μ L, concentration at which no inhibition of amoeba growth occurred).^{34,35} The stock solutions (1 mg/mL) of the compounds were freshly prepared and two-fold serial dilutions were made in the wells of a 96-well microtiter plate. The following controls were included in each plate: metronidazole as a standard amoebicidal drug, control wells (culture medium plus amoebae) and a blank (culture medium only). All the experiments were carried out in triplicate at each concentration and repeated thrice. The amoeba suspension was prepared from a confluent culture by pouring off the medium at 37 °C and adding 5 mL of fresh medium, chilling the culture tube on ice to detach the organisms from the side of the flask. The number of amoeba/ml was estimated with a haemocytometer, using the Trypan blue exclusion assay to confirm viability. The suspension was diluted to 10⁵ organism per mL in fresh medium and 170 μ L of this suspension was added to the test and control wells in the plate such that an inoculum of 1.7 \times 10⁴ organisms/well was achieved to ensure confluency, but no excessive growth in the control wells. Plates were sealed and gassed for 10 minutes with nitrogen before incubation at 37 °C for 72 h. After incubation, the growth of amoeba in the plate was checked with a low power microscope. The culture medium was removed by inverting the plate and shaking gently. The plate was then immediately washed with prewarmed (37 °C) 0.9% (w/v) sodium chloride solution. This procedure was completed as quickly as possible to ensure the plate did not cool, in order to prevent the detachment of amoebae. The plate was allowed to dry at room temperature and the amoebae were fixed with chilled (-20 °C) 100% methanol and then dried, stained with 0.5% aqueous eosin for 15 minutes. The stained plate was washed three times with distilled water and allowed to dry before 200 μ L 0.1 N sodium hydroxide was added to each well to dissolve the protein and release the dye. The optical density of the resulting solution was determined at 490 nm with a microplate reader. The % inhibition of amoebal growth was calculated taking into account the controls and then plotted against the logarithm of the compound concentration. Linear regression analysis was used to determine the best fitting line from which the IC₅₀ value was found.

4.3. *In vitro* antimalarial assay

Antimalarial activity of the compounds, against the chloroquine-resistant (FCR-3) strain of *P. falciparum*, was performed using the [³H]-hypoxanthine incorporation assay.¹⁶ The FCR-3 strain was continuously maintained *in vitro* in supplemented RPMI-1640 culture media and at a haematocrit of 5%. The culture was incubated at 37 °C in a gaseous atmosphere of 5% CO₂, 3% O₂, 92% N₂ and synchronized at the ring stage with 5% D-sorbitol before being adjusted to a final parasitemia of 0.5% and haematocrit of 1%.¹⁷ This suspension (200 μ L) was added to each well of the 96-well plate with the exception of four wells which received non-parasitized red blood cells. Stock solutions of the test compounds were made up in DMSO and serially diluted in culture medium in a 96-well microtiter plate.¹⁶ The microtiter plate was then incubated for 24 h. Following the incubation period, 25 μ L of the radiolabeled [³H]-hypoxanthine isotope (Amersham) at a concentration of 1.85 μ Ci/well was added to

each well. The microtiter plate was then incubated for a further 24 h. The parasitic DNA was harvested onto glass fibre filter mats by use of a Titertek™ semi-automatic cell harvester. The mats were then transferred to sample bags containing scintillation fluid (Wallac®) and the β -radioactivity counted on the Wallac® 1205 Betaplate scintillation counter. The counts per minute (cpm) were generated and the % parasite growth calculated. The concentration required to inhibit parasite growth by 50% (IC₅₀ value) was determined from log sigmoidal dose response curves using the GraphPad Prism® 5.0 software. Quinine a clinically used anti-malarial agent was used as the positive control. Each experiment was repeated, at least, in triplicate.

4.4. Inhibition of β -haematin formation assay

To determine whether the compounds had a similar mechanism of action to that of chloroquine, the following were combined in a 96-well microtiter plate: 25 μ L of the test compound, 25 μ L of a 1 mg/mL haemin (Sigma) solubilised in DMSO, 50 μ L H₂O and finally 100 μ L of a 0.5M acetate buffer. The acetate buffer was utilized to simulate the acidic conditions (pH 4.7) of the parasitic food vacuole. The plates were then incubated for 24 h and 100 μ L of the solution removed and the same volume substituted with DMSO, the plates were then centrifuged at 1500 g for 10 min. This was repeated 3 times to remove any unreacted haemin. Following this, 100 μ L was removed and substituted with a 2M NaOH solution to dissolve the β -haematin crystals. The solution was diluted twofold and the absorbance read at 405 nm.¹⁷ From the data obtained the concentration at which β -haematin formation was inhibited by 50% (IC₅₀ value) was determined using GraphPad Prism® 5.0 software. Each experiment was repeated at least in triplicate.

4.5. MTT cell viability assay

A human colon adenocarcinoma (HT29) cell line was cultured and maintained as a monolayer in Dulbecco's modified Eagle's medium (DMEM, Sigma) supplemented with 10% fetal calf serum (Sigma) and antibiotics (100 IU/mL of penicillin and 100 μ g/mL of streptomycin, Sigma). All cells were cultured at 37 °C in a humid atmosphere and 5% CO₂.¹⁸ Exponentially growing viable cells were plated at 0.15 \times 10⁶ cells per well into 96-well plates and incubated along with the test and control compounds. Stock solutions of compounds were initially dissolved in DMSO and all compounds screened at 100 μ M, where the final 1% DMSO in the well did not adversely affect cell growth. The growth-inhibitory effects of the compounds and positive control camptothecin were measured using the tetrazolium MTT assay. After 46 h of incubation at 37 °C, the medium was removed and 20 μ L of MTT (5 mg/mL in phosphate buffered saline (pH 7.4)) was added to each well. The plates were incubated at 37 °C for 2 h. At the end of the incubation period, the medium was removed and 150 μ L DMSO added to all wells. The metabolised MTT product dissolved in DMSO was quantified by reading the absorbance at 540 nm with a reference wavelength of 690 nm. All assays were performed at least in triplicate. Percent cell viability of the treated cells was calculated as a percentage of the untreated control cells taking into account the reference wavelength and cell free controls.

4.6. Red blood cell toxicity assay

The haemolytic activities of the compounds were evaluated in comparison to the standard antimalarial agent, quinine.¹⁹ A suspension of fresh human red blood cells was adjusted to a 1% haematocrit in culture media and plated together with each

test compound (100 μ M). This suspension was incubated for 48 h at 37 °C before the absorbance was read at 414 nm. The % haemolysis was calculated using a 2.0% (v/v) Triton X100 solution as the 100% haemolytic control. These results were used to generate a log sigmoid dose-response curve to calculate IC₅₀ values and the mean \pm s.d. were calculated from at least triplicate values.

4.7. X-ray Crystal Structure determination

Three-dimensional X-ray data for F7 was collected on a Bruker SMART Apex CCD diffractometer at 100(2) K, using a graphite monochromator and Mo-K α radiation ($\lambda = 0.71073$ Å) by the ϕ - ω scan method. Reflections were measured from a hemisphere of data collected of frames each covering 0.3 degrees in ω . Of the 20403 reflections measured in F7, all of which were corrected for Lorentz and polarization effects, and for absorption by semi-empirical methods based on symmetry-equivalent and repeated reflections, 2244 independent reflections exceeded the significance level $|F|/\sigma(|F|) > 4.0$. Complex scattering factors were taken from the program package SHELXTL³⁶. The structures were solved by direct methods and refined by full-matrix least-squares methods on F2. The non-hydrogen atoms were refined with anisotropic thermal parameters in all cases. The hydrogen atoms were located in difference Fourier map and freely refined. A final difference Fourier map showed no residual density outside: 0.533 and -0.392 e.Å⁻³ for F7. A weighting scheme $w = 1/[\sigma^2(F_o^2) + (0.061900P)^2 + 0.497700P]$ for F7, where $P = (|F_o|^2 + 2|F_c|^2)/3$, were used in the latter stages of refinement. CCDC 911483 contains the supplementary crystallographic data for the structure reported in this paper. These data can be obtained free of charge via <http://www.ccdc.cam.ac.uk/conts/retrieving.html>, or from the Cambridge Crystallographic Data Centre, 12 Union Road, Cambridge CB2 1EZ, UK; fax: (+44) 1223 336 033; or e-mail: deposit@ccdc.cam.ac.uk.

4.8. Homology modelling of Plasmodium falciparum dihydropteroate synthase (PfDHPS)

In *P. falciparum*, the two enzymes 7,8-dihydro-6-hydroxymethylpterin pyrophosphokinase (PPPK) and dihydropteroate synthase (DHPS), coexist as PPPK–DHPS bifunctional enzyme.³⁷ Therefore in the present study the amino acid sequence corresponding to PfDHPS, which ranges from 337 to 706 amino acid sequence was retrieved (Accession: Q27865) for homology modelling. Thereafter, homologous sequences were detected using PDB database²⁴ and 1TX0 (dihydropteroate synthetase, from *Bacillus anthracis*) was selected as the template based on the higher sequence identity/similarity. The template and the target sequence were then aligned and the alignment contains residues numbered 387 to 617 of the PfDHPS. Thus residues 387 and 617 served as the start and end of the modelled structure as the template X-ray crystal structure (1TX0) does not contain the equivalent amino acids for the remaining residues. Automated homology model building was performed using protein structure modelling program Modeller9v9.²⁵ Initially, 1000 models were generated which were then ranked individually on the basis of molpdf and DOPE scores respectively. We then selected 20 best models for each score and predicted the quality of the structure using PROCHECK²⁶ and VERIFY3D.²⁸ The model with the best quality was used for further refinement. Once the initial model was selected, we refined the loop regions (53-56, 77-88 and 149-155) using loop refinement module in MODELLER. Finally, explicit hydrogen's were added to the protein followed by its energy

minimization in Swiss PDB viewer.³⁸ The goodness of the predicted PfDHPS model was then assessed using PROCHECK and VERIFY3D. Further, in order to assess the reliability of the modelled structure of PfDHPS, we calculated the root mean square deviation (RMSD) by superimposing it on the known template structure.

4.9. Molecular docking

To determine the key residues that interact with the sulfonamide active site of the PfDHPS, the biomolecular interactions between the inhibitors (F7 and F8) and modeled PfDHPS was analyzed using Autodock 4.2.³⁰ Active site was obtained by structural superimposition of modeled PfDHPS with that of *E. coli* DHPS (Pdb id: 1AJ0). The crystal structure 1AJ0 was used for structural imposition as it contains sulfonamide bound in the active site. Docking simulations were performed using Lamarckian Genetic algorithm (LGA). The grid maps representing the ligand were calculated with Autogrid. The dimensions of the grid were 60 x 60 x 60 grid points with a spacing of 0.375 Å between the grid points and centered on the ligand (41.92, 8.09 and 1.876 coordinates). In the present study docking was performed by creating an initial population of 150 individuals, maximum number of evaluation 250000, maximum number of generations 27000, rate of gene mutation 0.02, cross-over rate 0.8 and the remaining parameters were set as default. 10 docking conformations (poses) were generated and the best docked conformation was selected based on the Autodock binding energy, for further analysis. Finally, Ligplot³¹ was used to map the hydrogen and hydrophobic interaction of the docked inhibitor to the modeled structure.

Acknowledgments

This work was supported by Council of Scientific and Industrial Research (Grant # 01(2278)/08/EMR-II New Delhi, India) and the Faculty of Health Sciences of the University of the Witwatersrand, South Africa.

References and notes

1. Monzote, L.; Siddiq, A. *The Open Medicinal Chemistry Journal* **2011**, 5, 1.
2. Collins, W. E.; Jeffery, G. M. *Clin. Microbiol. Rev.* **2007**, 20, 579.
3. a) Azam, A.; Agarwal, S. M. *Current Bioactive Compounds* **2007**, 3, 121. b) Agarwal, S. M.; Jain, R.; Bhattacharya, A.; Azam, A. *Int. J. Parasitol.* **2008**, 38, 137.
4. Muregi, F. W.; Ishih, A. *Drug Development Research* **2010**, 71, 20.
5. Garner, P.; Graves, P. M. *PLoS Med.* **2005**, 2, e105.
6. Araujo, N. C.; Barton, V.; Jones, M.; Stocks, P. A.; Ward, S. A.; Davies, J.; Bray, P. G.; Shone, A. E.; Cristiano, M. L.; O'Neill, P. M. *Bioorg. Med. Chem. Lett.* **2009**, 19, 2038.
7. a) Dechy-Cabaret, O.; Benoit-Vical, F.; Robert, A.; Meunier, B. *ChemBioChem* **2000**, 1, 281. b) Basco, L. K.; Dechy-Cabaret, O.; Ndounga, M.; Meche, F.S.; Robert, A.; Meunier, B. *Antimicrob. Agents Chemother.* **2001**, 45, 1886. c) Robert, A.; Dechy-Cabaret, O.; Cazelles, J.; Meunier, B. *Acc. Chem. Res.* **2002**, 35, 167. d) Meunier, B. *Acc. Chem. Res.* **2008**, 41, 69.
8. Bellot, F.; Cosledan, F.; Vendier, L.; Brocard, J.; Meunier, B.; Robert, A. *J. Med. Chem.* **2010**, 53, 4103.
9. a) Pérez, B.; Teixeira, C.; Gut, J.; Rosenthal, P. J.; Gomes, J. R.; Gomes, P. *ChemMedChem* **2012**, 7, 1537. b) October, N.; Watermeyer, N. D.; Yardley, V.; Egan, T. J.; Ncokazi, K.; Chibale, K. *ChemMedChem* **2008**, 3, 1649. c) Burgess, S. J.; Selzer, A.; Kelly, J. X.; Smilkstein, M. J.; Riscoe, M. K.; Peyton, D. H. *J. Med. Chem.* **2006**, 49, 5623. d) Eric, M.; Ncokazi, G. K.; Egan, T. J.; Gut, J.; Rosenthal, P. J.; Bhampidipati, R.; Kopinathan, A.; Smith, P. J.; Chibale, K. *J. Med. Chem.* **2011**, 54, 3637.
10. Hong, Y. L.; Hossler, P. A.; Calhoun, D. H.; Meshnick, S. R. *Antimicrob Agents Chemother.* **1995**, 39, 1756.

11. Hitchings, G. H. *Journal of Infectious Diseases*. **1973**, 128, S433.
12. Boison, J. O.; Nachilobe, P.; Cassidy, R.; Keng, L.; Thacker, P.A.; Peacock, A.; Fesser, A. C.; Lee, S.; Korsrud, G.O.; Bulmer, W. S. *Can. J. Vet. Res.* **1996**, 60, 281.
13. Tekwani, B. L.; Walker, L. A. *Comb Chem High Throughput Screen.* **2005**, 8, 63.
14. Marciniak, K.; Maślankiewicz, A.; Nowak, M.; Kusz, J. *Acta Cryst.* **2012**, 68, o2826.
15. Wright, C.W.; O'Neill, M. J.; Phillipson, J. D.; Warhurst, D. C. *Antimicrob. Agents Chemother.* **1988**, 32, 1725.
16. Desjardins, R. E.; Canfield, C. J.; Haynes, J. D.; Chulay, J. D. *Antimicrob. Agents Chemother.* **1979**, 16, 710.
17. Chemaly, S. M.; Chen, C. T.; van Zyl, R. L. *J. Inorg. Biochem.* **2007**, 101, 764.
18. Mosmann, T. J. *Immunol. Methods* **1983**, 65, 55.
19. Hayat, F.; Moseley, E.; Salahuddin, A.; Van Zyl, R. L.; Azam, A. *Eur. J. Med. Chem.* **2011**, 46, 1897.
20. Utukan, H.; Swaan, P. W. *Drugs*, **2002**, 62, 2039.
21. a) Lipinski, C. A.; Lombardo, F.; Dominy, B. W.; Feeney, P. J. *Adv. Drug Deliv. Rev.* **1997**, 23, 3. b) Lipinski, C. A. *Drug Discovery Today: Technologies* **2004**, 1, 337.
22. a) Veber, D. F.; Johnson, S.R.; Cheng, H. Y.; Smith, B. R.; Ward, K. W.; Kopple, K. D. *J. Med. Chem.* **2002**, 45, 2615. b) Andrews, P. R.; Craik, D. J.; Martin, J. L. *J. Med. Chem.* **1984**, 27, 1648. c) Refsgaard, H. H. F.; Jensen, B. F.; Brockhoff, P. B.; Padkjaer, S. B.; Guldbrandt, M.; Christensen, M. S. *J. Med. Chem.* **2005**, 48, 805.
23. Muegge, I. *Med. Res. Rev.* **2003**, 23, 302.
24. Berman, H. M.; Westbrook, J.; Feng, Z.; Gilliland, G.; Bhat, T. N.; Weissig, H.; Shindyalov, I. N.; Bourne, P. E. *Nucleic Acids Res.* **2000**, 28, 235.
25. Sali, A.; Blundell, T. L. *J. Mol. Biol.* **1993**, 234, 779.
26. Laskowski, R. A.; MacArthur, M. W.; Moss, D. S.; Thornton, J. M. *J. App. Cryst.* **1993**, 26, 283.
27. Salahuddin, A.; Agarwal, S. M.; Avecilla, F.; Azam, A. *Bioorg. Med. Chem. Lett.* **2012**, 22, 5694.
28. Lüthy, R.; Bowie, J. U.; Eisenberg, D. *Nature* **1992**, 5, 83.
29. Wiederstein, M.; Sippl, M. J. *Nucleic Acids Res.* **2007**, 35, W407.
30. Morris, G. M.; Huey, R.; Lindstrom, W.; Sanner, M. F.; Belew, R. K.; Goodsell, D. S.; Olson, A. J. *J. Comput. Chem.* **2009**, 30, 2785.
31. Wallace, A. C.; Laskowski, R. A.; Thornton, J. M. *Protein Engg.* **1995**, 8, 127.
32. Korsinczky, M.; Fischer, K.; Chen, N.; Baker, J.; Rieckmann, K.; Cheng, Q. *Antimicrob. Agents Chemother.* **2004**, 48, 2214.
33. Diamond, L. S.; Harlow, D. R.; Cunnick, C. C. *Trans. R. Soc. Trop. Med. Hyg.* **1978**, 72, 431.
34. Gillin, F. D.; Reiner, D. S.; Suffness, M. *Antimicrob. Agents Chemother.* **1982**, 22, 342.
35. Keene, A. T.; Harris, A.; Phillipson, J. D.; Warhurst, D. C. *Planta Med.* **1986**, 52, 278.
36. Sheldrick, G.M. SHELXL-97: An Integrated System for Solving and Refining Crystal Structures from Diffraction Data (Revision 5.1); University of Göttingen, Germany, 1997
37. Triglia, T.; Cowman, A.F. *Proc. Natl. Acad. Sci. USA.* **1994**, 91, 7149.
38. Guex, N.; Peitsch, M.C. *Electrophoresis*, **1997**, 18, 2714.